Mitochondrial Dysfunction and Increased Reactive Oxygen Species Impair Insulin Secretion in Sphingomyelin Synthase 1-null Mice*[S]

Masato Yano[‡1], **Ken Watanabe**[§], **Tadashi Yamamoto**[‡¶], **Kazutaka Ikeda**[‖], **Takafumi Senokuchi**[**], **Meihong Lu**[‡‡], **Tsuyoshi Kadomatsu**[‡], **Hiroto Tsukano**[‡], **Masahito Ikawa**[§§], **Masaru Okabe**[§§], **Shohei Yamaoka**[¶¶], **Toshiro Okazaki**[¶¶], **Hisanori Umehara**[‖‖], **Tomomi Gotoh**[‡], **Wen-Jie Song**[‡‡], **Koichi Node**[¶], **Ryo Taguchi**[‖], **Kazuya Yamagata**[**], and **Yuichi Oike**[‡2]

From the Departments of [‡]Molecular Genetics, [**]Medical Biochemistry, and [‡‡]Sensory and Cognitive Physiology, Faculty of Life Sciences, Kumamoto University, Kumamoto 860-8556, Japan, the [§]Department of Bone & Joint Disease, National Center for Geriatrics & Gerontology, Aichi 474-8511, Japan, the [¶]Department of Cardiovascular and Renal Medicine, Saga University, Saga 849-8501, Japan, the [‖]Department of Metabolome, Graduate School of Medicine, University of Tokyo, Tokyo 113-0033, Japan, the [§§]Research Institute for Microbial Diseases and Pharmaceutical Sciences, Osaka University, Osaka 565-0871, Japan, the [¶¶]Division of Clinical Laboratory Medicine and Hematology/Oncology, Faculty of Medicine, Tottori University, Tottori 683-8503, Japan, and the [‖‖]Department of Hematology and Immunology, Kanazawa Medical University, Ishikawa 920-0293, Japan

Sphingomyelin synthase 1 (SMS1) catalyzes the conversion of ceramide to sphingomyelin. Here, we generated and analyzed SMS1-null mice. SMS1-null mice exhibited moderate neonatal lethality, reduced body weight, and loss of fat tissues mass, suggesting that they might have metabolic abnormality. Indeed, analysis on glucose metabolism revealed that they showed severe deficiencies in insulin secretion. Isolated mutant islets exhibited severely impaired ability to release insulin, dependent on glucose stimuli. Further analysis indicated that mitochondria in mutant islet cells cannot up-regulate ATP production in response to glucose. We also observed additional mitochondrial abnormalities, such as hyperpolarized membrane potential and increased levels of reactive oxygen species (ROS) in mutant islets. Finally, when SMS1-null mice were treated with the anti-oxidant N-acetyl cysteine, we observed partial recovery of insulin secretion, indicating that ROS overproduction underlies pancreatic β-cell dysfunction in SMS1-null mice. Altogether, our data suggest that SMS1 is important for controlling ROS generation, and that SMS1 is required for normal mitochondrial function and insulin secretion in pancreatic β-cells.

Sphingolipids are important for stabilizing membrane structure (1, 2), cell-to-cell recognition, and signaling (3, 4). Some intermediates of sphingolipid metabolism function as second messengers in angiogenesis, cell growth, differentiation, and apoptosis (5–7). One intermediate, ceramide, is a key metabolite in both anabolic and catabolic pathways of sphingolipids (8), and it reportedly mediates cell differentiation, stress responses, and apoptosis (2). The function of ceramide in apoptosis is clinically significant, because many cancer chemotherapies apparently induce ceramide-dependent apoptosis (9–11). Although perturbation of ceramide homeostasis is related to many diseases, the function of ceramide in these conditions remains uncharacterized.

Sphingolipids are synthesized vectorially in cells. The initial step involves condensation of serine and a fatty acyl-Co-A, generating ceramide in the endoplasmic reticulum (ER),[3] followed by a series of reactions (supplemental Fig. S1) (12, 13). Newly synthesized ceramide is then transported from the ER to the Golgi complex by ceramide transfer protein, CERT (14, 15). Ceramide is converted to sphingomyelin by sphingomyelin synthase 1 (SMS1) in the Golgi complex (13, 16). Sphingomyelin is then transferred to the plasma membrane by exocytic vesicles and reversibly converted into ceramide by sphingomyelin synthase 2 (SMS2) on the plasma membrane.

Recently, several investigators have used mutant mice to analyze ceramide trafficking. CERT mutant mice exhibit embryonic lethality attributable to mitochondrial degeneration (17). CERT importance has also been demonstrated in *Drosophila melanogaster,* in which CERT-null flies exhibit a higher oxidative stress response and a shortened lifespan (18). SMS2 mutant mice exhibit an attenuated inflammatory response in macrophages (19) and reduced sphingomyelin levels in plasma and liver (20). However, the effect of SMS1 ablation *in vivo* has not been examined, although it has been analyzed in cultured cells in which investigators found that SMS1 plays a critical role in proliferation of mouse lymphoid cells (16). Membrane sphingomyelin is reportedly important for Fas clustering through aggregation of lipid rafts, leading to

[3] The abbreviations used are: ER, endoplasmic reticulum; CERT, ceramide transfer protein; SMS1, sphingomyelin synthase 1; ROS, reactive oxygen species; GTT, glucose tolerance test; ITT, insulin tolerance test; NAC, N-acetyl cysteine; KO, knock-out; WAT, white adipose tissue.

Fas-mediated apoptosis (21). Suppression of SMS1 also results in enhanced ceramide production and apoptosis after photodamage (22).

Here, we generated SMS1 knock-out (SMS1-KO) mice. They exhibited moderate neonatal lethality, reduced body weight, and loss of fat tissues mass, suggesting that they might have metabolic abnormality. Then, we first analyzed glucose metabolism of the mice, and found that SMS1-KO mice showed severe deficiencies in insulin secretion. Therefore, in this study, we focused on the analysis to reveal the reason why insulin secretion was reduced in SMS1-KO mice. Isolated SMS1-KO islets exhibited severe deficiency in insulin release dependent on glucose stimuli. SMS1-KO islet mitochondria showed abnormalities, such as decreased ATP production, hyperpolarized membrane potential, and increased ROS. These results suggest that increased ROS production followed by mitochondrial dysfunction impairs insulin secretion in SMS1-KO mice. Strikingly, insulin release deficiency was rescued when SMS1-KO mice were supplied an anti-oxidant reagent, suggesting that ROS over-production underlies mitochondrial dysfunction of SMS1-KO pancreatic β-cells. Altogether, our data suggest that SMS1 is important for controlling ROS generation, and that SMS1 is required for normal mitochondrial function and normal insulin secretion in pancreatic β-cells.

EXPERIMENTAL PROCEDURES

Materials and Reagents—All reagents were supplied by Sigma-Aldrich or Wako (Osaka, Japan), unless otherwise stated. Urinary 8-hydroxydeoxy-guanosine (8-OHdG) levels were measured using an ELISA kit (Nikken Seil, Shizuoka, Japan). *N*-[7-(4-nitrobenzo-2-oxa-1,3-diazole)]-6-aminocaproyl-D-erythro-sphingosine (C_6-NBD-ceramide) was purchased from Cayman Chemical (Ann Arbor, MI).

Generation of SMS1-KO Mice—Genomic DNA clones of the *Sms1* locus were isolated from a mouse 129/Svj genomic library (Stratagene, Santa Clara, CA) using full-length Sms1 cDNA as a probe. Exon 2, which encodes the translation initiation codon, the SAM domain and two SMS1 transmembrane regions, was replaced with a neo cassette. An 8-kbp EcoRI fragment containing the intron between exons 2 and 3 as a long arm and a 1 kbp EcoRI/PstI fragment of regions upstream of exon 2 as a short arm were inserted into pPGKneo(wt). The gene encoding the diphtheria toxin A fragment (DT-A) from pMC1-DT-A was inserted into the end of the long arm as a negative selection marker. The targeting vector was linearized, electroporated into D3 embryonic stem (ES) cells, and clones were selected in G418. Targeting events were screened by PCR and confirmed by Southern blot analysis. Recombinant cells were karyotyped to ensure that 2N chromosomes were present in most metaphase spreads. Chimeric mice derived from correctly targeted ES cells were mated with C57BL/6 mice to obtain F1 $Sms1^{+/-}$ mice. All experiments were performed using F3 generation mice. PCR primers used to distinguish targeted from wild-type alleles were: GOR2SAp3, 5′-TTTGAGGAGAGAGGCCTTGAGTCTC-3′; GOR2-R1, 5′-AGGCAGCCACTTCCAGCAGCCAG-3′; and PGKneoS, 5′-TCGCCTTCTATCGCCTTCTTGAC-3′.

GOR2SAp3 and GOR2-R1 primers amplified a 381 bp DNA fragment from the wild-type allele, whereas GOR2SAp3 and PGKneoS primers amplified a 552-bp fragment from the targeted allele. PCR was carried out with 30 cycles consisting of 94.5 °C, 1 min; 60 °C, 1 min; 72 °C, 1 min.

Long and Accurate (LA)-PCR—To confirm the homologous recombination, PCR was performed. For detection short arm, KOD-Fx (TOYOBO, Osaka, Japan) was used according to the manufacturer's protocol. The primer sequences are as follows; (a) GOR2-SA1, 5′-GGGCTATCAGAAACTTCTTGATG-3′, (b) GOR2-R1, 5′-AGGCAGCCACTTCCAGCAGCCAG-3′, (c) PGKneoS, 5′-TCGCCTTCTATCGCCTTCTTGAC-3′. Long-accurate (LA)-PCR was performed for confirm the recombination in long arm. The protocol for the LA-PCR is as follows; an initial denature step, 95 °C, 1 min; 30 cycles of 98 °C, 10 s and 68 °C, 15 min, using LA-Taq (TAKARA, Kyoto, Japan). The primers used are as follows; (d) GOR2WT-LA-2F, 5′-GAG-TGGTTTCCTGGTGTTGGATAAAGTC-3′, (e) NML1, 5′-GCCTACCCGCTTCCATTGCTCAGC-3′, (f) GOR2-FLA-2R, 5′-CCTGTTTAGAGCTTCGTCTCTTACTC-3′.

Northern Blotting—Total RNA was isolated from embryonic fibroblasts using RNeasy kit (Qiagen, Valencia, CA). Ten micrograms of total RNA were electrophoresed and blotted onto nylon membrane. The hybridization was performed using full-length (FL) or a PCR fragment (ex2) corresponding to SAM domain of mouse SMS1 cDNA as a ^{32}P-labeled probe. The washed membranes were exposed to imaging plates, and the signals were developed by BAS2000 system (Fujifilm, Tokyo, Japan).

TLC Analysis of Sphingomyelin Synthase (SMS) and Glycosylceramide Synthase (GCS) Activity—Genes for wild-type SMS1 and mutant SMS1 (SMS1 Δex2), in which exon 2 region encoding the translation initiation codon, the SAM domain and two SMS1 transmembrane regions was deleted, were transducted in WR19L/Fas-SM(−) cells by retro virus system (16). The cells were homogenized in an ice-cold buffer containing 20 mM Tris-HCl, pH 7.4, 2 mM EDTA, 10 mM EGTA, 1 mM phenylmethylsulfonyl fluoride, and 2.5 μg/ml leupeptin. The lysates containing 100 μg of cell protein were added to a reaction solution containing 10 mM Tris-HCl, pH 7.5, 1 mM EDTA, 20 μM C_6-NBD-ceramide, 120 μM phosphatidylcholine (PC), and incubated at 37 °C for 60 min. The lipids were extracted by the method of Bligh and Dyer (23), applied on the thin-layer chromatgraphy (TLC) plates, and developed with solvent containing chloroform/methanol/12 mM MgCl$_2$ in H$_2$O (65:25:4). The fluorescent lipids were visualized by LAS-1000 system (Fujifilm).

Animal Studies—Animals were housed in a temperature-controlled room with a 12-h light/dark cycle. Food and water were available *ad libitum* unless noted. Mice were fed a normal diet (CE-2; CLEA, Japan). NAC (40 mM) was administered in drinking water. All experimental protocols were approved by the Ethics Review Committee for Animal Experimentation of Kumamoto University.

Metabolic Measurements—Glucose tolerance test (GTT) and insulin tolerance test (ITT) were performed as described (24). For GTT, mice were deprived of food for 16 h and injected intraperitoneally with 1 mg/kg glucose. For ITT, mice

were administered 1 unit/kg of human insulin by intraperitoneal injection. Blood was withdrawn from the supraorbital plexus at times indicated in figures. Blood glucose was measured using the glucose oxidase method (Sanwa Kagaku, Nagoya, Japan), and serum insulin was measured by using an ELISA kit (Morinaga Institute of Biological Science, Yokohama, Japan).

Morphological Analysis of Pancreatic Islets—Pancreas tissues isolated from wild-type or mutant mice were fixed in 4% paraformaldehyde, and random sections were generated. Islet number per unit area of pancreas and islet size were measured using hematoxylin-eosin-stained sections. For immunohistochemistry, sections were incubated with anti-insulin guinea pig IgG (Affinity BioReagents, Rockford, IL) and anti-glucagon rabbit polyclonal antibody (Thermo Scientific, Waltham, MA) at 1:200 dilutions. Samples were then incubated in Alexa Fluor 647-labeled goat anti-guinea pig IgG and Alexa Fluor 488-labeled goat anti-rabbit IgG (Molecular Probes, Eugene, OR). Immunofluorescence for insulin and glucagon was observed using a Biorevo BZ-9000 fluorescence microscope (Keyence, Osaka, Japan).

Isolation of Pancreatic Islets—Mouse pancreatic islets were isolated by collagenase digestion as described (25, 26) with slight modification. Mice were anesthetized by intraperitoneal injection of thiopental sodium. Collagenase (collagenase type S-1, 0.6 mg/ml; Nitta Gelatin, Osaka, Japan) was dissolved in Hanks' Balanced Salt Solutions (Sigma) with 800 KI units/ml aprotinin (Wako). Collagenase solution was injected into the common bile duct. Pancreata were dissected and incubated in collagenase solution at 37 °C for 20 min with shaking. The solution was then mixed with ice-cold isotonic sucrose buffer and chilled on ice for 20 min. Precipitated islets were collected for further experiments.

Quantitative RT-PCR—Total RNA from islet tissues was isolated with TRIzol reagent (Invitrogen), and DNase-treated RNA was reverse transcribed with a PrimeScript RT reagent kit (Takara Bio, Osaka, Japan), following the manufacturer's protocol. PCR products were analyzed using a Thermal Cycler Dice Real Time system (Takara Bio), and transcript abundance was normalized to that of β-actin mRNA. PCR oligonucleotides and gene abbreviations are listed in supplemental Table S1.

Measurement of Insulin Release from Islets—Groups of 10–15 islets were incubated for 1 h in Ca^{2+}-containing HEPES-added Krebs-Ringer bicarbonate buffer (HKRB) solution (129 mM NaCl, 1.2 mM $MgSO_4$, 1.2 mM KH_2PO_4, 4.7 mM KCl, 5 mM $NaHCO_3$, 2.5 mM $CaCl_2$, 10 mM HEPES, pH7.4, with 0.05% bovine serum albumin) with 2.2 mM glucose at 37 °C under 5% CO_2 atmosphere stabilization, followed by test incubation for 1 h in HKRB with 2.2 or 22 mM glucose. The concentration of secreted insulin was determined by using an ELISA kit (Medical & Biological Laboratories).

Measurement of ATP Levels, Mitochondrial Membrane Potential, and ROS Production—To measure ATP content in islet cells, groups of 20–30 islets were incubated for 1 h in HKRB with 2.2 mM or 22 mM glucose at 37 °C. ATP in islets was extracted in 0.1% trichloroacetic acid and neutralized in 0.1 M Tris acetate. ATP levels were measured using a Cellular ATP Assay Kit (Toyo Ink, Tokyo, Japan) using Luminometer Model TD-20/20 (Promega, San Luis Obispo, CA). To measure mitochondrial membrane potential, groups of 20–30 islets were loaded with JC-1 (Invitrogen, Carlsbad, CA) by incubation in HKRB with 2.2 or 22 mM glucose at 37 °C for 1 h. Red and green fluorescence was observed under a fluorescence microscope. Red fluorescence was also monitored in a plate-reader fluorometer, Fluoroskan Ascent (Thermo Labsystem, Helsinki, Finland). To measure ROS production in islets, groups of 20–30 islets were incubated in HKRB with 2.2 mM glucose in the presence of $CM-H_2DCFDA$ (Invitrogen). Green fluorescence derived from ROS generation was monitored in a plate-reader fluorometer.

Isolation of Pancreatic Mitochondria—Mitochondria were isolated as described (27, 28) with minor modifications. Pancreas tissues were isolated and minced in mitochondria isolation buffer (3 mM HEPES-KOH, pH 7.5, 210 mM mannitol, 70 mM sucrose, 0.2 mM EGTA) containing a protease inhibitor mixture (Roche, Basel, Switzerland). Samples were disrupted using a tissue grinder (Iwaki, Tokyo, Japan), and homogenates were centrifuged at 500 × *g* for 5 min to remove nuclei and unbroken cells followed by centrifugation at 10,000 × *g* for 5 min to obtain the mitochondrial pellet. The pellet was suspended in mitochondria isolation buffer and purified by consecutive centrifugations (500 × *g* for 5 min twice to recover the supernatant and at 10,000 × *g* three times to recover the pellet). All procedures were performed under ice-cold conditions.

Sphingolipid Extraction and LC/ESI-MS Analysis—Total lipids from islets or pancreas mitochondria from wild-type and SMS1-KO mice were extracted with 1 ml methanol for 1 h at room temperature. In this process, 1 nmol of sphingomyelin (d18:1/12:0) and ceramide (d18:1/12:0) were added as internal standards. Extracts were centrifuged at 10000 × *g* for 15 min, and the supernatant was collected and re-dissolved with chloroform:methanol (2:1; v/v) after drying under a gentle nitrogen stream. LC/ESI-MS analysis was performed using a quadrapole/time of flight hybrid mass spectrometer (Q-TOF micro) with an ACQUITY UPLC system (Waters Corp., Milford, MA). The scan range was set at *m/z* 200–1100 and scan duration of MS and MS/MS at 0.5 s in negative ion mode (29, 30). The capillary voltage was set at 2.5 kV, cone voltage at −30 V and collision energy for MS/MS analysis at −30 V. Reverse-phased LC separation was achieved using an ACQUITY UPLC BEH C18 column (1.0 × 150 mm i.d., Waters Corporation) at 45 °C. 2 μl of total lipids normalized to protein content were individually injected. The mobile phase was acetonitrile/methanol/water (19/19/2) (0.1% formic acid + 0.028% ammonia) (*A*), and isopropanol (0.1% formic acid + 0.028% ammonia) (*B*), and the composition was produced by mixing these solvents. The gradient consisted of holding in (A/B: 90/10) solvent for 7.5 min, and then linearly converting to solvent (A/B: 70/30) for 32.5 min and finally converting to solvent (A/B: 40/60) for 50 min. The mobile phase was pumped at a flow rate of 40–50 μl/min. MS data processing was applied using Mass++ software to detect each chromatogram peak with quantitative accuracy.

Immunoblot Analysis—Isolated islets were solubilized in PBS containing 1% SDS. Total protein was separated by SDS-PAGE, transferred to nitrocellulose membranes, and analyzed with ECL Western blotting Detection Reagents (GE Healthcare, Buckinghamshire, England). Immunoblotting was performed with anti-Hsc70 antibody (Santa Cruz Biotechnology, Santa Cruz, CA), anti-4-hydroxy-2-nonenal (4-HNE) antibody (R&D Systems, Minneapolis, MN), anti-Complex I NDUFA9 (αs9) antibody (Invitrogen), anti-Complex II 70 kDa subunit (Fp) antibody (Invitrogen), or anti-Complex III subunit core 2 (QCR2) antibody (Invitrogen).

Statistical Analysis—Data were analyzed using Student's t test and reported as means ± S.E., unless stated. Indicated significance levels are: *, $p < 0.05$; **, $p < 0.01$; ***, $p < 0.001$.

RESULTS

Targeted Disruption of SMS1 Gene Eliminate SMS1 Activity—To analyze the effect of SMS1 ablation *in vivo*, we generated SMS1-null (SMS1-KO) mice (Fig. 1). Exon 2 of *SMS1* gene, which encodes the translation initiation codon, the SAM domain and two transmembrane regions, was replaced with a neo cassette (Fig. 1*A*). The allele, designated SMS1-KO, was established and confirmed by LA-PCR (Fig. 1*B*). Deletion of the region corresponding to exon 2 in SMS1 mRNA derived from SMS1-KO mice was confirmed by northern-blot analysis (Fig. 1*C*). To confirm that this SMS1-KO construct, which may express N-terminal deletion mutant of SMS1 (SMS1Δex2), does not exhibit sphingomyelin synthase (SMS) activity, we measured SMS activity of SMS1Δex2 in SMS activity null cells (Fig. 1*D*). Although wild-type SMS1 produce a significant amount of sphingomyelin (SM) derivative (NDB-SM), SMS1Δex2 did not, suggesting that SMS1Δex2 has no SMS activity. Thus, we concluded that the activity of SMS1 was completely disrupted in SMS1-KO mice used in this study. Conventionally, we used PCR technique to distinguish wild-type, heterozygous, and KO mice (Fig. 1*E*).

SMS1-KO Mice Exhibit Reduced Insulin Secretion—We initially observed growth of SMS1-KO mice. They showed moderate neonatal lethality with half of mice dead by 10 weeks (Fig. 2*A*), suggesting that SMS1 gene is important for normal growth of mice. And, we found that the body weight of SMS1-KO mice was reduced (Fig. 2*B*). To investigate the reason, we anatomically analyzed and found that the mass of white adipose tissue (WAT) was significantly reduced (Fig. 2*C*). These results suggested that SMS1-KO mice might have metabolic deficiency.

Then, we next examined the possibility whether blood glucose homeostasis was affected by SMS1 ablation. Blood tests indicated that SMS1-KO mice exhibited hyperglycemia after 16 h of fasting, suggesting impaired glucose homeostasis (Fig. 2*D*). Glucose tolerance tests (GTT) further indicated that glucose uptake of SMS1-KO mice was impaired (Fig. 2*E*). Analysis of insulin in serum samples obtained from GTTs showed that glucose-induced insulin release was significantly reduced in SMS1-KO mice (Fig. 2*F*). However, SMS1-KO mice exhibited higher insulin sensitivity compared with wild-type mice based on insulin tolerance tests (ITT) (Fig. 2*G*). Therefore, we concluded that lower glucose uptake seen in SMS1-KO mice

was due to impaired insulin secretion. In the following experiments, we focused on the analysis to reveal the reason why insulin secretion was reduced in SMS1-KO mice.

Pancreatic β-cell Death Does Not Underlie Insulin Secretion Deficiencies Seen in SMS1-KO Mice—Because SMS1 ablation will enhance accumulation of ceramide, an enzymatic substrate of SMS1, we first measured the amount of sphingolipid species in SMS1-KO islets by LC/ESI-MS analysis (Fig. 3, *A*–*C*). As expected, the amount of sphingomyelin species was reduced (Fig. 3*A*), whereas the amount of ceramide species was increased in SMS1-KO islets (Fig. 3*B*). The amount of phosphatidylcholine, another substrate of SMS1, seemed to be a little increased (about 1.2-fold), but the increment was not significant (data not shown). The amount of GM3, a glycosphingolipid, was also increased (Fig. 3*C*), suggesting that accumulated ceramide species were alternatively metabolized into glycosphingolipid species. However, we could not find any significant change of expression of mRNAs for sphingolipid metabolisms (Fig. 3*D* and supplemental Fig. S1 and Table S1).

Because ceramide reportedly promotes cell death (31, 32), we estimated that loss of insulin secretion in SMS1-KO mice might be attributable to ceramide-induced death of pancreatic β-cells. To test this possibility, we examined expression of mRNAs related to apoptosis. However, no significant changes were observed in expression of apoptosis-inducing factors (Bax and CHOP) or apoptosis-inhibiting factors (Bip, Bcl-2, Bcl-X and Mcl-1) (Fig. 3*E* and supplemental Table S1). In addition, we observed no difference in islet size (Fig. 3*F*), density (Fig. 3*G*), or morphology (Fig. 3, *H* and *I*). These results suggest that pancreatic β-cell death does not underlie the insulin secretion deficiency seen in SMS1-KO mice.

SMS1-KO Islets Exhibit Decreased Insulin Secretion Accompanied by Mitochondrial Abnormalities—To determine the primary cause of insulin secretion deficiency seen in SMS1-KO mice, we asked whether insulin secretion was reduced in SMS1 deficient islets. First, by an ELISA, we confirmed that the total amount of insulin in isolated SMS1-KO islets was equivalent to that seen in wild-type islets (Fig. 4*A*). When islets were incubated under high glucose (22 mM) conditions, SMS1-KO islets released only low levels of insulin, whereas wild-type islets released large amounts (Fig. 4*B*). Thus, we concluded that insulin secretion deficiency observed in SMS1-KO mice was attributed to insulin secretion deficiency of pancreatic β-cells.

Because SMS1 resides in the Golgi complex, we hypothesized that other intracellular organelles might be damaged by SMS1 deletion. Indeed, intracellular levels of ceramide in ER and mitochondria are reportedly increased when the ceramide transfer protein, CERT, is ablated (17). Then, we focused in particular on the effect of SMS1 loss on mitochondria, because mitochondria are important for insulin secretion (33, 34). Mitochondria were highly purified from pancreas (supplemental Fig. S2). Analysis using LC/ESI-MS revealed that the amounts of some kinds of sphingomyelin species were reduced in pancreatic mitochondria of SMS1-KO mice (Fig. 4*C*), whereas some kinds of ceramide
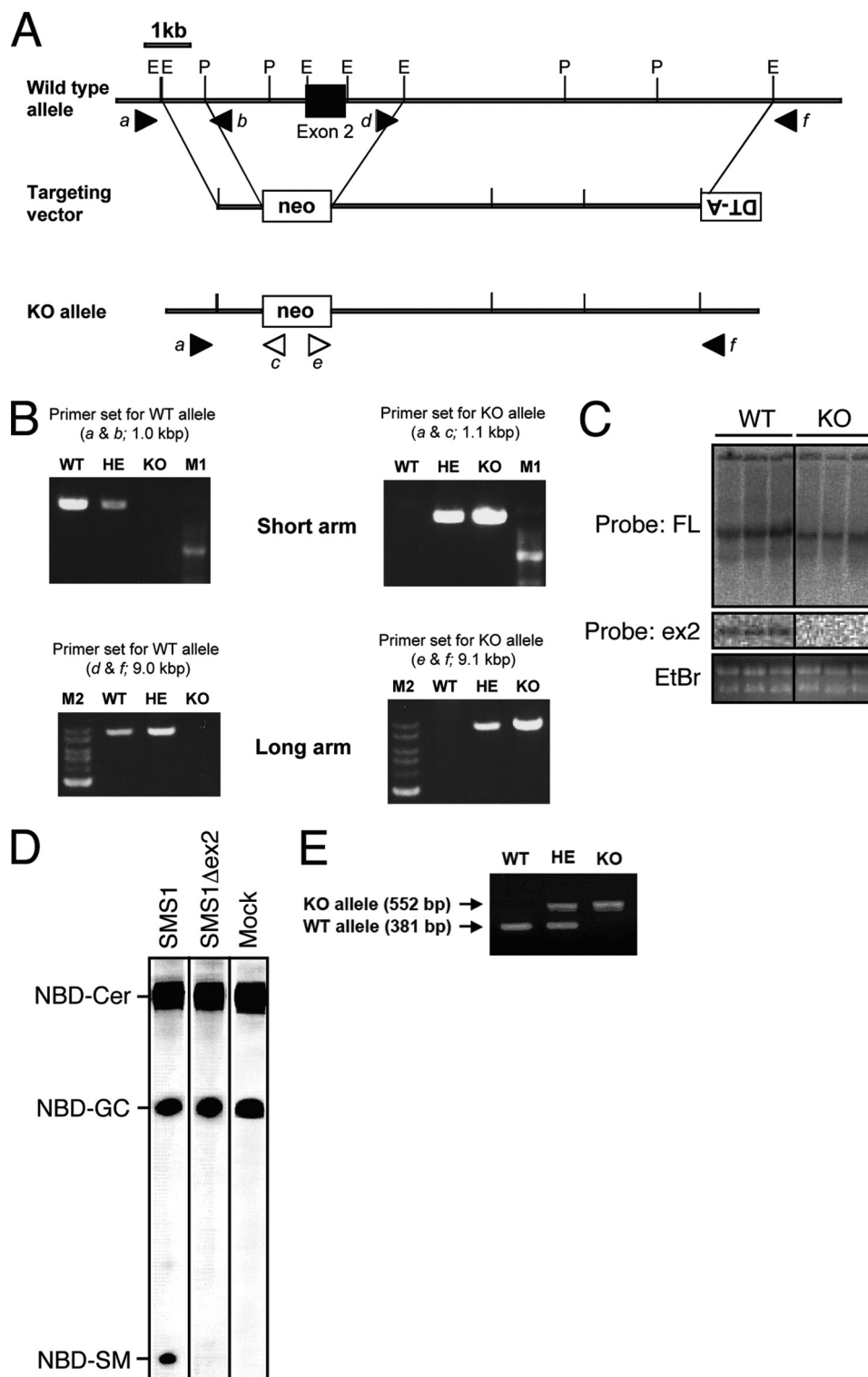
FIGURE 1. **Construction and confirmation of SMS1-KO mice.** *A*, schematic representation of the targeting vector, the wild-type *Sms1* locus, and the mutant allele after homologous recombination. Exon 2 is denoted by *filled boxes*. E and P represent EcoRI and PstI restriction sites, respectively. *Closed* and *open arrowheads* are corresponding to the primer position to detect WT and KO alleles, respectively. Primer sequences are shown in "Experimental Procedures." *B*, confirmation of homologous recombination by PCR. *Upper two panels* show the amplified PCR fragments for WT or KO allele as indicated. A ladder is 100-bp DNA marker (M1). *Lower two panels* show the amplified fragments by LA-PCR. The ladders shown *left* in each panel are of 1-kb DNA ladder (M2). Primer set (*e.g. a & b*) for each PCR is shown in *A*. *C*, Northern blot analysis. The results of three each of total RNA was independently isolated from WT or KO. *Top* and *middle panels* showed the hybridized bands detected by full-length cDNA probe (*FL*) and exon 2 probe (*ex2*), respectively. *Bottom panel* showed total RNA stained by ethidium bromide (*EtBr*). *D*, SMS activity of SMS1 and SMS1Δex2. Genes for wild-type SMS1 and mutant SMS1 (SMS1 Δex2), in which exon 2 region encoding the translation initiation codon, the SAM domain and two SMS1 transmembrane regions was deleted in the same manner as SMS1-KO mice, were transduced in SMS activity-null cells by retro virus system. The cell lysates were mixed with C_6-NBD-ceramide and PC and incubated at 37 °C for 60 min. The lipids were extracted and applied on the TLC plates. Mock indicates empty vector. *E*, confirmation of the genotype of newborn mice by PCR. Primer sequences are shown in "Experimental Procedures."
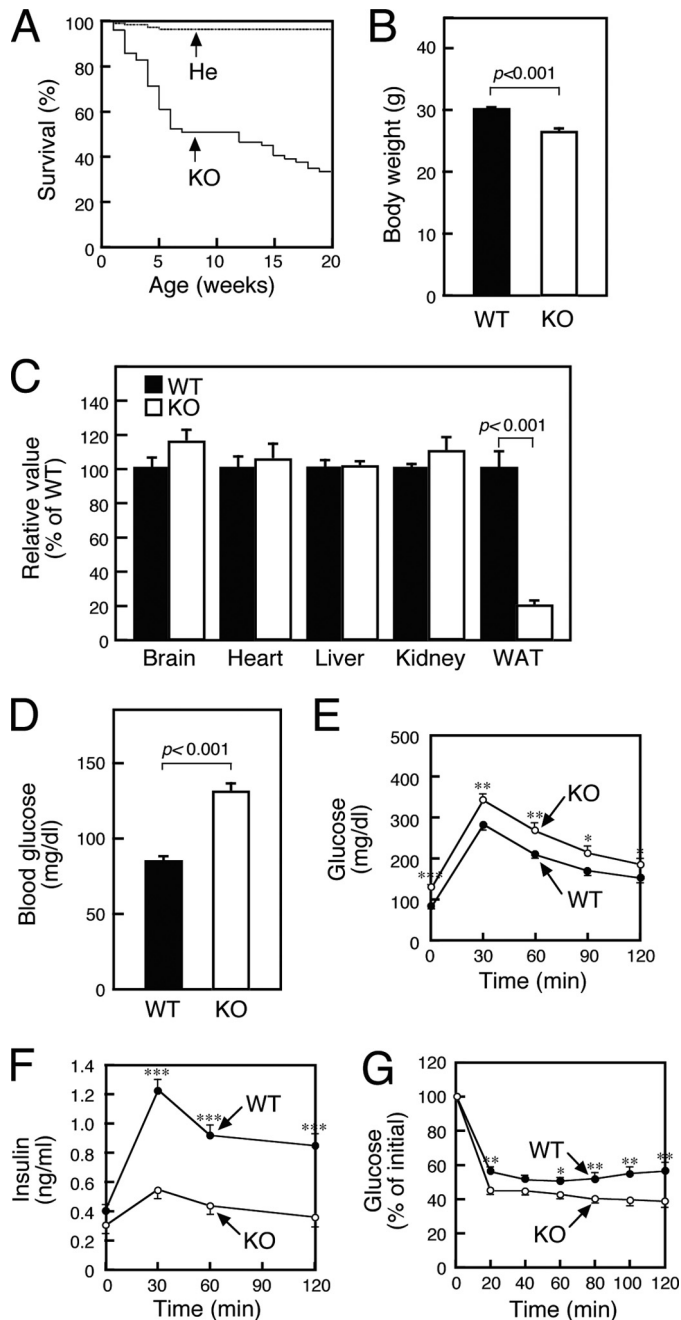
FIGURE 2. **SMS1-KO mice exhibit reduced insulin secretion.** *A*, survival curve of SMS1-KO (*KO*, $n = 68$) and heterozygous (*He*, $n = 153$) mice. *B*, body weights of 10 weeks old wild-type (*WT*, $n = 37$) and SMS1-KO mice (*KO*, $n = 9$). *C*, weight of organs of 10-week-old mice (*WT*, $n = 6$; *KO*, $n = 4$). Mice of 12–16 weeks old were used for the following analysis. *D*, blood glucose levels after 16 h of fasting were measured using the glucose oxidase method (*WT*, $n = 21$; *KO*, $n = 20$). *E*, glucose tolerance tests. Mice were deprived of food for 16 h and injected with 1 mg/kg glucose. Blood was withdrawn at times indicated, and blood glucose was measured (*WT*, $n = 21$; *KO*, $n = 24$). *F*, amounts of insulin in the serum obtained from glucose tolerance tests performed in *E* were measured by an ELISA (*WT*, $n = 32$; *KO*, $n = 25$). *G*, insulin tolerance test. Mice were administered 1 unit/kg of human insulin. Blood was withdrawn at times indicated, and blood glucose was measured (*WT*, $n = 21$; *KO*, $n = 20$). *, $p < 0.05$; **, $p < 0.01$; ***, $p < 0.001$.

species were increased (Fig. 4*D*), suggesting that SMS1-KO mitochondria might exhibit dysfunction.

Because mitochondrial activation and up-regulated ATP synthesis are key steps in insulin secretion (33, 34), we ana-

lyzed islet ATP content (Fig. 4*E*). When islets were incubated in low glucose (2.2 mM) condition, no significant difference in ATP content was observed between wild-type and SMS1-KO islets. However, when islets were incubated in high glucose (22 mM) condition, SMS1-KO islets exhibited significantly lower ATP content relative to wild-type islets, indicating that the mitochondria of SMS1-KO pancreatic β-cells have deficiency to synthesize ATP in response to glucose stimulation.

To analyze other mitochondrial anomalies in SMS1-KO pancreatic β-cells, we used the fluorescent dye JC-1 (5′5′6′6′-tetrachloro-1′1″3′3′-tetraethylbenzimidazolylcarbocyanine iodide) to detect mitochondrial membrane potential. JC-1 gives red fluorescence when mitochondrial membrane potential is high, whereas it gives green fluorescence when the potential is low. We found that SMS1-KO islets showed significantly stronger red fluorescence, indicative of increased membrane potential, than did wild-type islets (Fig. 4*F*). Higher mitochondrial membrane potential observed in SMS1-KO islets was seen in both low and high glucose conditions (Fig. 4*G*).

Because SMS1-KO islet exhibited higher mitochondrial membrane potential but lower ATP synthesis, we estimated that the mitochondrial respiratory complex in SMS1-KO pancreatic β-cells cannot transport electrons efficiently, and that breakdown in electron transport may increase ROS production. Indeed, it is reported that increased mitochondrial ceramide directly inhibits mitochondrial respiratory complex III, leading to ROS generation (35–37). Thus, we measured ROS levels in islets using the ROS-reactive fluorescent reagent, 5-(and-6)-chloromethyl-2′,7′-dichlorodihydrofluorescein diacetate, acetyl ester (CM-H$_2$DCFDA) (Fig. 4*H*). As predicted, ROS levels in SMS1-KO islets were significantly greater than that seen in wild-type cells. Immunoblot analysis of islets and pancreas using anti-4-hydroxy-2-nonenal (4-HNE) antibody, which recognizes ROS-modified proteins, also indicated that ROS levels in SMS1-KO islets and pancreas were significantly greater than that seen in wild-type (Fig. 4*I*). Additionally, 8-hydroxydeoxyguanosine (8-OHdG), a marker of ROS generation, was also increased in the urine of SMS1-KO mice, suggesting that ROS generation increases systemically in SMS1-KO mice (Fig. 4*J*). Because excessive ROS production in mitochondria induce oxidative modification of mitochondrial lipids, proteins, and DNA (38–40), mitochondrial respiration complex components of SMS1-KO islet could be damaged by excessive ROS.

Expression of Mitochondrial Respiratory Complex Components Is Enhanced in SMS1-KO Islets—If mitochondrial proteins, especially mitochondrial respiratory complex components, were damaged by ROS, mRNAs encoding mitochondrial respiratory complex components might be up-regulated to compensate for damage. To examine this possibility, we performed real-time-PCR analysis of islet tissues to assay expression of mRNAs encoding respiratory complex components. These transcripts were up-regulated in SMS1-KO islet cells relative to wild-type cells (Fig. 5*A* and supplemental Table S1). Such increases were particularly significant for mRNAs encoding proteins of Complex I, which is a major source of ROS. Indeed, immunoblot analysis revealed
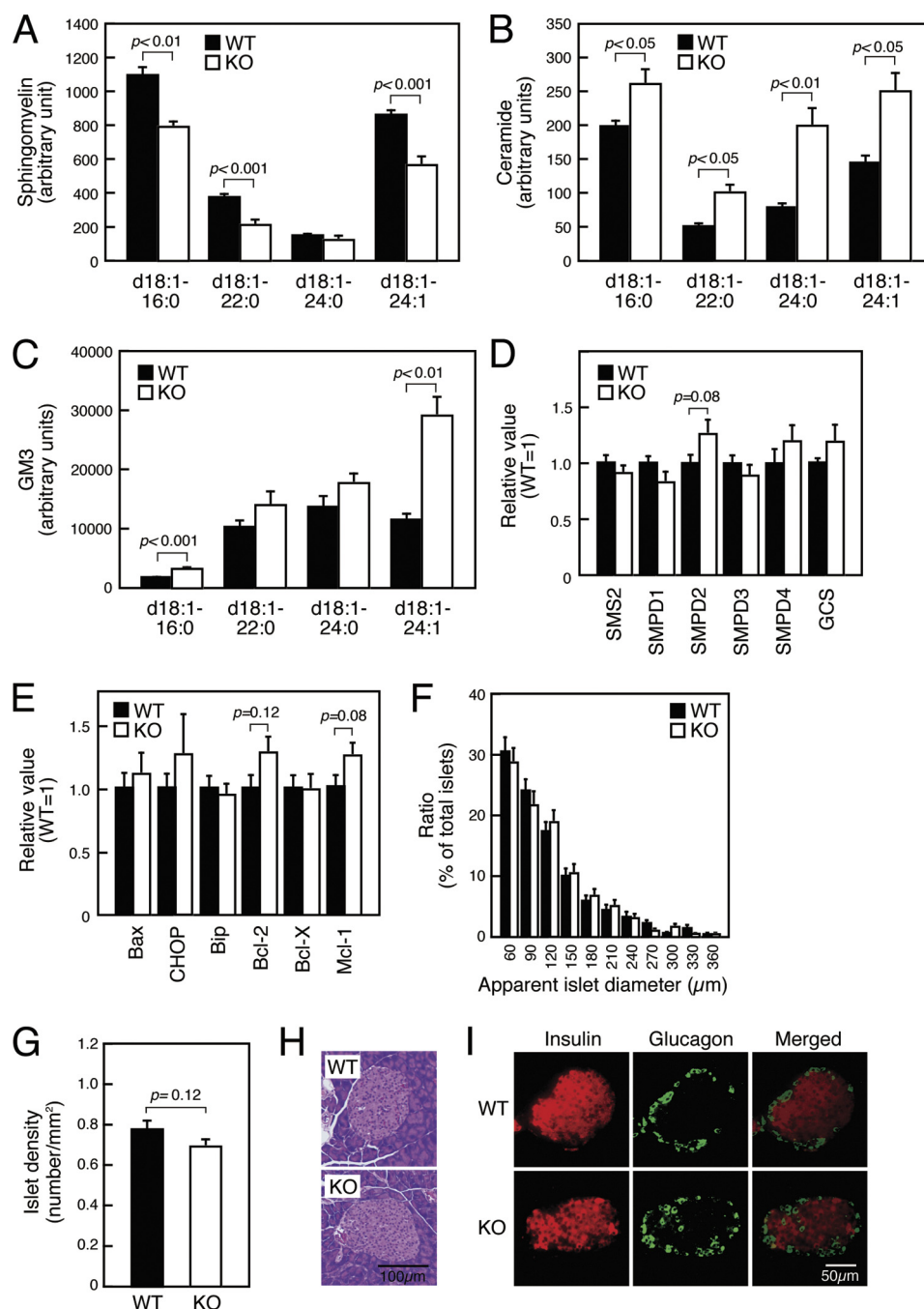
FIGURE 3. **Pancreatic β-cell death is not a cause of insulin secretion deficiency seen in SMS1-KO mice.** Mice, 12–16 of weeks old, were used for analysis. *A–C*, Levels of sphingomyelin (*A*), ceramide (*B*), GM3 (*C*) species in pancreatic islets was measured by LC/ESI-MS. Islets isolated from three mice of the same genotype constituted one sample. $n = 4$ samples per group. *D*, expression levels of genes for sphingolipid metabolism were assessed by quantitative RT-PCR. Islets isolated from two mice of the same genotype served as one sample. Individual measurements were normalized to β-actin expression, and the wild-type group average was set to 1. $n = 6-8$ samples per group. *E*, expression levels of genes encoding factors indicative of apoptosis were assessed by quantitative RT-PCR. $n = 8-12$ samples per group. *F*, apparent diameter of islets seen in cross section (*WT*, $n = 771$; *KO*, $n = 678$). *G*, number of islets per cross-section (*WT*, $n = 102$; *KO*, $n = 104$). *H*, histochemical analysis of islets by hematoxylin-eosin stain. *I*, immunohistochemical analysis of islets for insulin and glucagon.

that protein expression of αs9 (NDUFA9), a component of Complex I, was much higher in SMS1-KO islets (Fig. 5*B*). When expression of mRNAs encoding factors relevant to mitochondrial biogenesis was analyzed, mRNAs for peroxisome proliferator-activated receptor-γ (PPARγ) and PPARγ coactivators (PGC-1α and PGC-1β) were up-regulated in SMS1-KO islets (Fig. 5*C* and supplemental Table S1), possibly in response to mitochondrial dysfunction induced by ROS. In ad-

dition, mitochondrial uncoupling protein 2 (UCP2) was up-regulated in SMS1-KO islets, suggesting a compensatory response to ROS generation at the expense of decreased ATP production (Fig. 5*D* and supplemental Table S1). Expression of mRNAs encoding ROS detoxification enzymes, such as catalase, was also increased. Overall, these results suggest that major ROS-induced cell responses were enhanced in SMS1-KO islets.
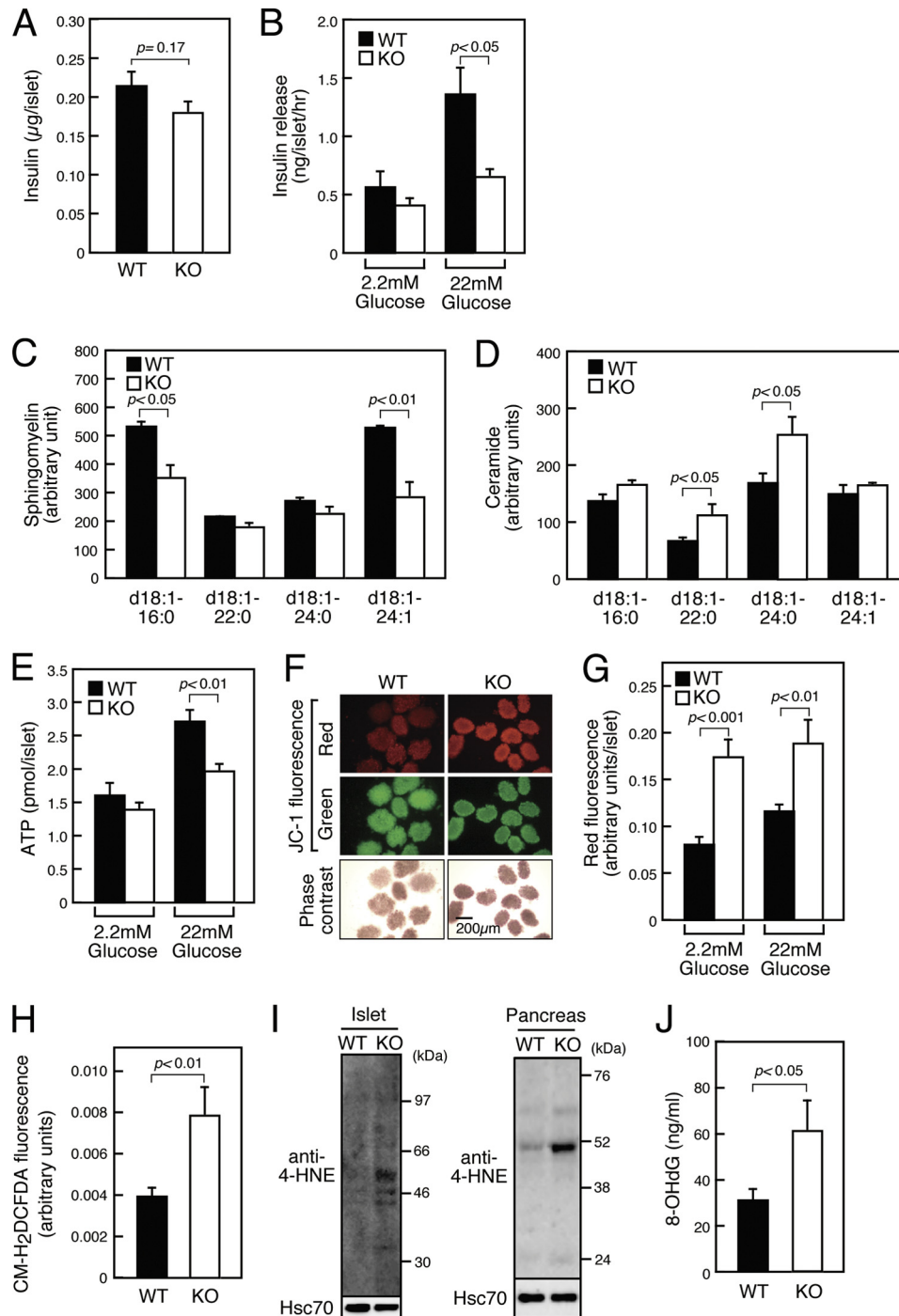
FIGURE 4. **SMS1-KO islets exhibit reduced insulin secretion accompanied by reduced ATP synthesis, increased mitochondrial membrane potential, and increased ROS generation.** Mice of 12–16-week-old were used for analysis. *A*, insulin content in islet protein extracts was examined by an ELISA (*WT*, $n = 10$; *KO*, $n = 6$). *B*, insulin release from isolated islets. Islets were incubated in the presence of 2.2 mm or 22 mm glucose, and released insulin was detected by an ELISA (*WT*, $n = 12$; *KO*, $n = 12$). *C* and *D*, levels of sphingomyelin (*C*) and ceramide (*D*) species in isolated pancreatic mitochondria was analyzed by LC/ESI-MS. $n = 3$ samples per group. *E*, total cellular ATP concentration in isolated islets was determined following a 1-h incubation period in 2.2 mm and 22 mm glucose (*WT*, $n = 16$; *KO*, $n > 15$). *F*, mitochondrial membrane potential was observed by assessing islets loaded with JC-1 following a 1 h-incubation period in 2.2 mm glucose. *G*, quantification of red fluorescence intensity in islets loaded with JC-1 following 1-h incubation in 2.2 mm or 22 mm glucose (*WT*, $n > 19$; *KO*, $n > 17$). *H*, detection of ROS generation using CM-H$_2$DCFDA-loaded islets after 1 h of incubation in 2.2 mm glucose (*WT*, $n = 15$; *KO*, $n = 12$). *I*, detection of ROS-modified proteins in islets (*left panel*) and pancreas (*right panel*) by anti-4-HNE antibody. *J*, concentration of urinary 8-OHdG, a marker of ROS generation (*WT*, $n = 10$; *KO*, $n = 8$).

Deficiencies in Glucose Homeostasis and Insulin Secretion in SMS1-KO Mice Is Partially Rescued by Anti-oxidant Treatment—Our results led us to hypothesize that increased ROS generation seen in SMS1-KO mice underlies the phenotypes seen in these mice and that treatment with anti-oxidants might rescue these conditions (Fig. 6). To test this idea, we supplied the anti-oxidant *N*-acetyl cysteine (NAC) in animal drinking water and then analyzed
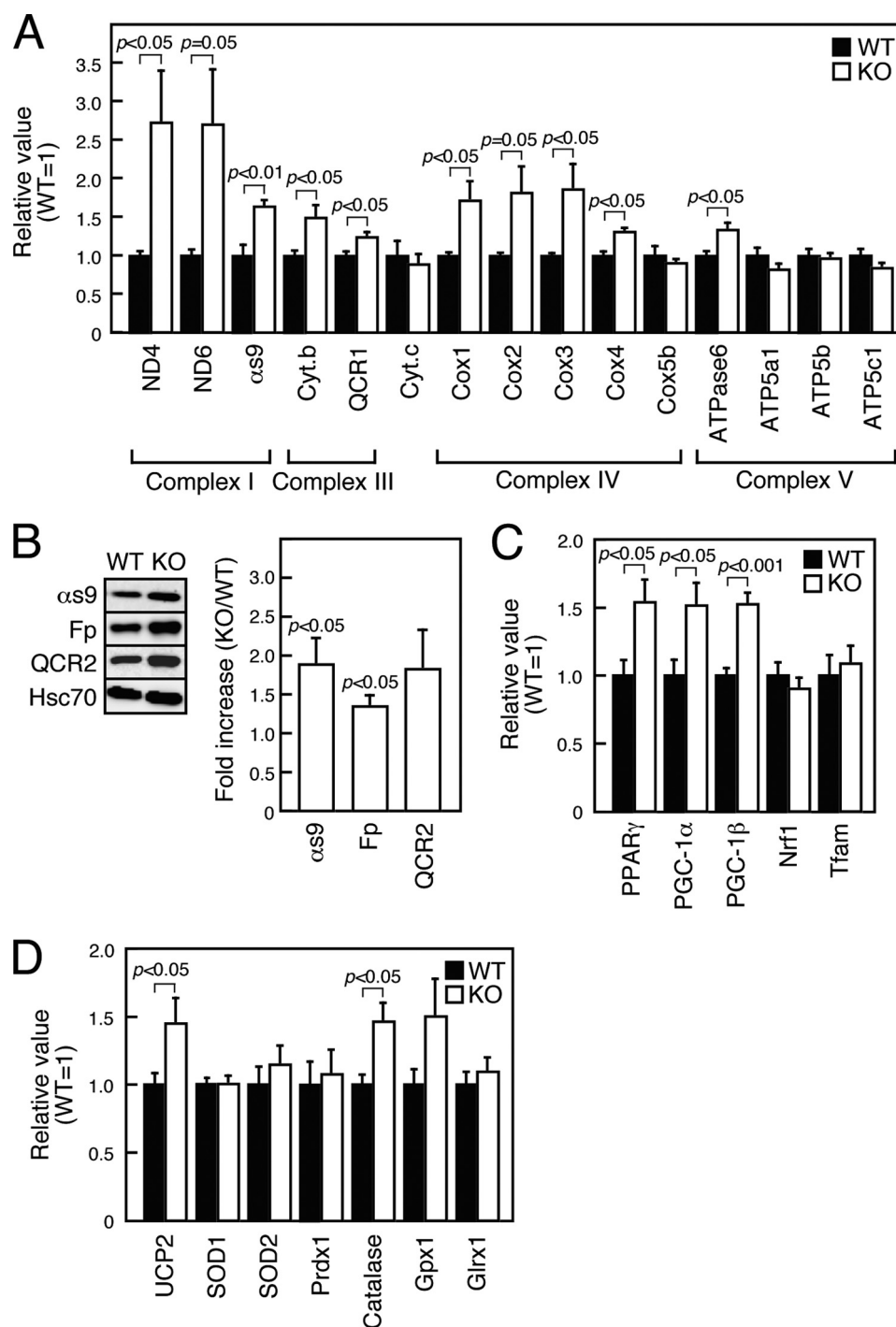
FIGURE 5. **Mitochondrial biogenesis is enhanced in SMS1-KO islets.** mRNA or protein expression in islets isolated from 12–16-week-old mice was examined by quantitative RT-PCR or immunoblot analysis, respectively. *A*, expression levels of genes encoding mitochondrial respiration complex factors were assessed. Islets isolated from two mice of the same genotype served as one sample. Individual measurements were normalized to β-actin expression, and the wild-type group average was set to 1. $n = 6–8$ samples per group. *B*, expression levels of mitochondrial respiration complex proteins were assessed by immunoblot analysis. Islets isolated from four mice of the same genotype constituted one sample. Individual measurements were standardized using Hsc70, and the wild-type group average was set to 1. Increases in ratio in KO *versus* WT are shown as *Fold increase*. $n = 3$ samples per group. *C*, expression levels of genes encoding mitochondrial biogenesis proteins were assessed. $n = 6–12$ samples per group. *D*, expression levels of genes encoding UCP2 and ROS detoxification enzymes were assessed. $n = 8–12$ samples per group.

urinary levels of 8-OHdG, a marker of ROS generation. NAC-treated SMS1-KO mice showed significantly decreased 8-OHdG levels compared with untreated SMS1-KO mice (Fig. 6*A*). Furthermore, NAC treatment improved glucose uptake and insulin secretion in

SMS1-KO mice (Fig. 6, *B* and *C*). Surprisingly, NAC-treated SMS1-KO mice showed reduced lethality (Fig. 6*D*). Overall, these results indicate that increased ROS production underlies insulin secretion deficiencies and lethality seen in SMS1-KO mice.
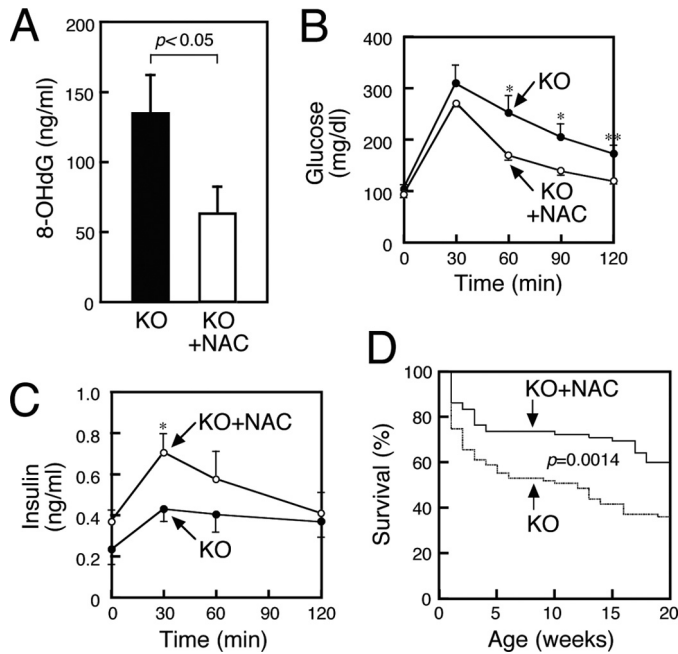
FIGURE 6. **NAC treatment improves deficiencies of glucose uptake and insulin secretion seen in SMS1-KO mice.** SMS1-KO mice supplied with normal (*KO*) or NAC-containing drinking water (*KO+NAC*) for 20–24 weeks were used for the following analysis. *A*, concentration of urinary 8-OHdG, a marker of ROS generation, was assessed (KO, $n = 8$; KO+NAC, $n = 10$). *B*, blood glucose levels based on glucose tolerance tests. Mice were deprived of food for 16 h and injected with 1 mg/kg glucose. Blood was withdrawn at times indicated. Blood glucose was measured using the glucose oxidase method (*KO*, $n = 7$; *KO+NAC*, $n = 7$). *C*, serum insulin levels derived from glucose tolerance tests. The amounts of insulin in the serum obtained from glucose tolerance tests performed in *B* were measured by an ELISA (*KO*, $n = 7$; *KO+NAC*, $n = 7$). *D*, survival curve of SMS1-KO supplied with normal (*KO*, $n = 87$) or NAC-containing drinking water (*KO+NAC*, $n = 72$). *, $p < 0.05$; **, $p < 0.01$.

DISCUSSION

Although investigators have examined SMS1 function in cell growth and apoptosis in cell culture, the significance of SMS1 loss *in vivo* has not been reported. Here, we generated SMS1-KO mice and found that SMS1-KO mice exhibited moderate neonatal lethality, reduced body weight, and loss of fat tissues mass, suggesting that they might have metabolic deficiency. We further found that they were hyperglycemic and showed insulin secretion deficiencies. The deficiencies were not attributable to death of pancreatic β-cells. Isolated SMS1-KO islets exhibited severely impaired ability to release insulin, dependent on glucose stimuli, indicating that impaired insulin secretion from pancreatic β-cells is a primary cause of insulin secretion deficiency observed in SMS1-KO mice. Therefore, in this study, we focused on analyzing how SMS1 deletion disturbs insulin secretion from pancreatic β-cells.

Lipid composition analysis revealed that the amount of sphingomyelin species was reduced whereas that of ceramide species was increased in SMS1-KO islet. These results appeared to be reasonable, because ceramide and sphingomyelin are enzymatic substrate and product of SMS reaction, respectively. However, reduction of the amounts of sphingomyelin in SMS1-KO islet appeared to be small. Although the reason is unclear, we consider that other sphingomyelin synthetic or influx pathway is present. For example, a portion of SMS2 may be reside in Golgi complex, and partially participate in sphingomelin synthesis in Golgi complex to compensate for SMS1 ablation. Alternatively, it is also possible that sphingomyelin, which is derived from food intake, flow into the cell by endocytosis.

Analysis of lipid content in pancreatic mitochondria indicated that the amount of sphingomyelin species was reduced in SMS1-KO mice, whereas that of ceramide species was increased. Indeed, intracellular levels of ceramide in ER and mitochondria are reportedly increased when the ceramide transfer protein, CERT, is ablated (17). These authors also found that mitochondrial ceramide accumulation is associated with mitochondrial degeneration, including the capacity to generate ATP. These conclusions are similar to our observations that SMS1-KO islets exhibited deficiencies in ATP production following glucose stimuli. In addition, mitochondria of SMS1-KO islet showed other anomalies, such as hyperpolarized membrane potential and increased ROS production. These results are consistent with previous reports indicating that increased ROS generation induced by knockdown of the mitochondrial ROS detoxification enzyme, nicotinamide nucleotide transhydrogenase (Nnt), uncouples mitochondrial metabolism of pancreatic β-cells, leading to impaired ATP production and insulin secretion deficiency (41, 42). In addition, we observed higher expression of genes encoding mitochondrial respiratory chain complex components and transcription factors related to mitochondrial biogenesis. Up-regulation of these genes suggests that functional proteins are newly synthesized to compensate for ROS damage. In particular, mitochondrial complex I was highly expressed in SMS1-KO islets, which may promote higher membrane potential and increased ROS generation, as reported (40, 43). UCP2 was also up-regulated in SMS1-KO islets, in agreement with reports suggesting that the ROS-damaged β-cells express UCP2 to antagonize ROS production in mitochondria (44, 45). Overall, we estimate that mitochondrial respiration complexes in β-cells are functionally damaged by increased ceramide species in SMS1-KO mice and that electron leakage generates ROS, further damaging the mitochondrial respiration machinery. We further estimate that mitochondrial respiration complex components are up-regulated to restore mitochondria damaged by ROS, and that UCP2 is up-regulated to reduce oxidative damage caused by ROS generation.

Finally, we found that the anti-oxidant NAC treatment improved glucose uptake and rescued insulin secretion deficiencies seen in SMS1-KO mice, supporting the idea that ROS production underlies insulin secretion deficiency seen in SMS1-KO pancreatic β-cells. These observations are noteworthy because these data suggest that increment of ceramide itself is not so much toxic, rather, the following ROS generation is very toxic. Altogether, our data suggest that SMS1 plays a critical role in regulating mitochondrial sphingolipid homeostasis and is required to control mitochondrial ATP and ROS production, which are important for insulin secretion in pancreatic β-cells.

Regulation of Insulin Secretion by SMS1

It is explicit that SMS1 is important for whole body health, because SMS1-KO mice exhibit moderate neonatal lethality. And, SMS1 appears to be important for suppressing onset of ROS-related diseases, because NAC treatment prolonged the lifespan of SMS1-KO mice. These observations are consistent with previous reports that ROS functions in cell senescence (46, 47) and that reduction of ROS by NAC extends lifespan (48). Anyway, further experiments are necessary to reveal the complicated relationship between SMS1 function and ROS-related disease.

In this study, we demonstrates that manipulation of sphingolipid flux *in vivo* and consequent ceramide accumulation in pancreatic β-cells leads to defects in insulin secretion by oxidative stress probably imposed on mitochondria. Overall, our approach identifies an essential role for SMS1 in insulin secretion and provides molecular insight into the role of the *de novo* sphingolipid biosynthetic pathway in regulating the ROS generation pathway, which is related to metabolic disease.

REFERENCES

1. Zeidan, Y. H., and Hannun, Y. A. (2007) *Trends Mol. Med.* **13,** 327–336
2. Hannun, Y. A., and Obeid, L. M. (2008) *Nat. Rev. Mol. Cell Biol.* **9,** 139–150
3. Futerman, A. H., and Hannun, Y. A. (2004) *EMBO Rep.* **5,** 777–782
4. Zheng, W., Kollmeyer, J., Symolon, H., Momin, A., Munter, E., Wang, E., Kelly, S., Allegood, J. C., Liu, Y., Peng, Q., Ramaraju, H., Sullards, M. C., Cabot, M., and Merrill, A. H., Jr. (2006) *Biochim. Biophys. Acta* **1758,** 1864–1884
5. Alvarez, S. E., Milstien, S., and Spiegel, S. (2007) *Trends Endocrinol. Metab.* **18,** 300–307
6. van Meer, G., Voelker, D. R., and Feigenson, G. W. (2008) *Nat. Rev. Mol. Cell Biol.* **9,** 112–124
7. Wymann, M. P., and Schneiter, R. (2008) *Nat. Rev. Mol. Cell Biol.* **9,** 162–176
8. Hannun, Y. A., Luberto, C., and Argraves, K. M. (2001) *Biochemistry* **40,** 4893–4903
9. Ogretmen, B., and Hannun, Y. A. (2004) *Nat. Rev. Cancer* **4,** 604–616
10. Swanton, C., Marani, M., Pardo, O., Warne, P. H., Kelly, G., Sahai, E., Elustondo, F., Chang, J., Temple, J., Ahmed, A. A., Brenton, J. D., Downward, J., and Nicke, B. (2007) *Cancer Cell* **11,** 498–512
11. Zeidan, Y. H., Jenkins, R. W., Korman, J. B., Liu, X., Obeid, L. M., Norris, J. S., and Hannun, Y. A. (2008) *Curr. Drug Targets* **9,** 653–661
12. Menaldino, D. S., Bushnev, A., Sun, A., Liotta, D. C., Symolon, H., Desai, K., Dillehay, D. L., Peng, Q., Wang, E., Allegood, J., Trotman-Pruett, S., Sullards, M. C., and Merrill, A. H., Jr. (2003) *Pharmacol. Res.* **47,** 373–381
13. Tafesse, F. G., Ternes, P., and Holthuis, J. C. (2006) *J. Biol. Chem.* **281,** 29421–29425
14. Hanada, K., Kumagai, K., Yasuda, S., Miura, Y., Kawano, M., Fukasawa, M., and Nishijima, M. (2003) *Nature* **426,** 803–809
15. Hanada, K., Kumagai, K., Tomishige, N., and Yamaji, T. (2009) *Biochim. Biophys. Acta* **1791,** 684–691
16. Yamaoka, S., Miyaji, M., Kitano, T., Umehara, H., and Okazaki, T. (2004) *J. Biol. Chem.* **279,** 18688–18693
17. Wang, X., Rao, R. P., Kosakowska-Cholody, T., Masood, M. A., Southon, E., Zhang, H., Berthet, C., Nagashim, K., Veenstra, T. K., Tessarollo, L., Acharya, U., and Acharya, J. K. (2009) *J. Cell Biol.* **184,** 143–158
18. Rao, R. P., Yuan, C., Allegood, J. C., Rawat, S. S., Edwards, M. B., Wang, X., Merrill, A. H., Jr., Acharya, U., and Acharya, J. K. (2007) *Proc. Natl. Acad. Sci. U.S.A.* **104,** 11364–11369
19. Hailemariam, T. K., Huan, C., Liu, J., Li, Z., Roman, C., Kalbfeisch, M., Bui, H. H., Peake, D. A., Kuo, M. S., Cao, G., Wadgaonkar, R., and Jiang, X. C. (2008) *Arterioscler. Thromb. Vasc. Biol.* **28,** 1519–1526
20. Liu, J., Zhang, H., Li, Z., Hailemariam, T. K., Chakraborty, M., Jiang, K., Qiu, D., Bui, H. H., Peake, D. A., Kuo, M. S., Wadgaonkar, R., Cao, G., and Jiang, X. C. (2009) *Arterioscler. Thromb. Vasc. Biol.* **29,** 850–856
21. Miyaji, M., Jin, Z. X., Yamaoka, S., Amakawa, R., Fukuhara, S., Sato, S. B., Kobayashi, T., Domae, N., Mimori, T., Bloom, E. T., Okazaki, T., and Umehara, H. (2005) *J. Exp. Med.* **202,** 249–259
22. Separovic, D., Semaan, L., Tarca, A. L., Awad Maitah, M. Y., Hanada, K., Bielawski, J., Villani, M., and Luberto, C. (2008) *Exp. Cell Res.* **314,** 1860–1868
23. Okazaki, T., Bell, R. M., and Hannun, Y. A. (1989) *J. Biol. Chem.* **264,** 19076–19080
24. Oike, Y., Akao, M., Yasunaga, K., Yamauchi, T., Morisada, T., Ito, Y., Urano, T., Kimura, Y., Kubota, Y., Maekawa, H., Miyamoto, T., Miyata, K., Matsumoto, S., Sakai, J., Nakagata, N., Takeya, M., Koseki, H., Ogawa, Y., Kadowaki, T., and Suda, T. (2005) *Nat. Med.* **11,** 400–408
25. Wollheim, C. B., Meda, P., and Halban, P. A. (1990) *Methods Enzymol.* **192,** 188–223
26. Yamagata, K., Nammo, T., Moriwaki, M., Ihara, A., Iizuka, K., Yang, Q., Satoh, T., Li, M., Uenaka, R., Okita, K., Iwahashi, H., Zhu, Q., Cao, Y., Imagawa, A., Tochino, Y., Hanafusa, T., Miyagawa, J., and Matsuzawa, Y. (2002) *Diabetes* **51,** 114–123
27. Yano, M., Hoogenraad, N., Terada, K., and Mori, M. (2000) *Mol. Cell. Biol.* **20,** 7205–7213
28. Yano, M., Terada, K., Gotoh, T., and Mori, M. (2007) *Exp. Cell Res.* **313,** 3767–3778
29. Houjou, T., Yamatani, K., Imagawa, M., Shimizu, T., and Taguchi, R. (2005) *Rapid Commun. Mass. Spectrom.* **19,** 654–666
30. Ikeda, K., Oike, Y., Shimizu, T., and Taguchi, R. (2009) *J. Chromatogr. B. Analyt. Technol. Biomed. Life Sci.* **877,** 2639–2647
31. Hannun, Y. A. (1996) *Science* **274,** 1855–1859
32. Pettus, B. J., Chalfant, C. E., and Hannun, Y. A. (2002) *Biochim. Biophys. Acta* **1585,** 114–125
33. Maechler, P., and Wollheim, C. B. (2001) *Nature* **414,** 807–812
34. Wiederkehr, A., and Wollheim, C. B. (2006) *Endocrinology* **147,** 2643–2649
35. Gudz, T. I., Tserng, K. Y., and Hoppel, C. L. (1997) *J. Biol. Chem.* **272,** 24154–24158
36. García-Ruiz, C., Colell, A., Marí, M., Morales, A., and Fernández-Checa, J. C. (1997) *J. Biol. Chem.* **272,** 11369–11377
37. Morales, A., Lee, H., Goñi, F. M., Kolesnick, R., and Fernandez-Checa, J. C. (2007) *Apoptosis* **12,** 923–939
38. Choksi, K. B., Boylston, W. H., Rabek, J. P., Widger, W. R., and Papaconstantinou, J. (2004) *Biochim. Biophys. Acta* **1688,** 95–101
39. Balaban, R. S., Nemoto, S., and Finkel, T. (2005) *Cell* **120,** 483–495
40. Murphy, M. P. (2009) *Biochem. J.* **417,** 1–13
41. Freeman, H., Shimomura, K., Horner, E., Cox, R. D., and Ashcroft, F. M. (2006) *Cell Metab.* **3,** 35–45
42. Shimomura, K., Galvanovskis, J., Goldsworthy, M., Hugill, A., Kaizak, S., Lee, A., Meadows, N., Quwailid, M. M., Rydström, J., Teboul, L., Ashcroft, F., and Cox, R. D. (2009) *Methods Enzymol.* **457,** 451–480
43. Kussmaul, L., and Hirst, J. (2006) *Proc. Natl. Acad. Sci. U.S.A.* **103,** 7607–7612
44. Rousset, S., Alves-Guerra, M. C., Mozo, J., Miroux, B., Cassard-Doulcier, A. M., Bouillaud, F., and Ricquier, D. (2004) *Diabetes* **53,** Suppl. 1, S130–S135
45. Affourtit, C., and Brand, M. D. (2008) *Biochim. Biophys. Acta* **1777,** 973–979
46. Chen, Q., Fischer, A., Reagan, J. D., Yan, L. J., and Ames, B. N. (1995) *Proc. Natl. Acad. Sci. U.S.A.* **92,** 4337–4341
47. Hagen, T. M., Yowe, D. L., Bartholomew, J. C., Wehr, C. M., Do, K. L., Park, J. Y., and Ames, B. N. (1997) *Proc. Natl. Acad. Sci. U.S.A.* **94,** 3064–3069
48. Macip, S., Igarashi, M., Fang, L., Chen, A., Pan, Z. Q., Lee, S. W., and Aaronson, S. A. (2002) *EMBO J.* **21,** 2180–2188